Impact of a revised convective triggering mechanism on Community Atmosphere Model, Version 2, simulations: Results from short-range weather forecasts

Shaocheng Xie,[1] Minghua Zhang,[2] James S. Boyle,[1] Richard T. Cederwall,[1] Gerald L. Potter,[1] and Wuyin Lin[2]

Received 25 February 2004; revised 10 May 2004; accepted 18 May 2004; published 20 July 2004.

[1] This study implements a revised convective triggering condition in the National Center for Atmospheric Research (NCAR) Community Atmosphere Model, Version 2 (CAM2), model to reduce its excessive warm season daytime precipitation over land. The new triggering mechanism introduces a simple dynamic constraint on the initiation of convection that emulates the collective effects of lower level moistening and upward motion of the large-scale circulation. It requires a positive contribution from the large-scale advection of temperature and moisture to the existing positive convective available potential energy (CAPE) for model convection to start. In contrast, the original convection triggering function in CAM2 assumes that convection is triggered whenever there is positive CAPE, which results in too frequent warm season convection over land arising from strong diurnal variation of solar radiation. We examine the impact of the new trigger on CAM2 simulations by running the climate model in numerical weather prediction (NWP) mode so that more available observations and high-frequency NWP analysis data can be used to evaluate model performance. We show that the modified triggering mechanism has led to considerable improvements in the simulation of precipitation, temperature, moisture, clouds, radiations, surface temperature, and surface sensible and latent heat fluxes when compared to the data collected from the Atmospheric Radiation Measurement (ARM) Program at its Southern Great Plains (SGP) site. Similar improvements are also seen over other parts of the globe. In particular, the surface precipitation simulation has been significantly improved over both the continental United States and around the globe; the overestimation of high clouds in the equatorial tropics has been substantially reduced; and the temperature, moisture, and zonal wind are more realistically simulated. Results from this study also show that some systematic errors in the CAM2 climate simulations can be detected in the early stage of model integration. Examples are the extremely overestimated high clouds in the tropics in the vicinity of Intertropical Convergence Zone and the spurious precipitation maximum to the east of the Rockies. This has important implications in studies of these model errors since running the climate model in NWP mode allows us to perform a more in-depth analysis during a short time period where more observations are available and different model errors from various processes have not compensated for the systematic errors. *INDEX TERMS:* 0320 Atmospheric Composition and Structure: Cloud physics and chemistry; 1620 Global Change: Climate dynamics (3309); 3314 Meteorology and Atmospheric Dynamics: Convective processes; 3337 Meteorology and Atmospheric Dynamics: Numerical modeling and data assimilation; *KEYWORDS:* convective trigger, convection, CAM2

Citation: Xie, S., M. Zhang, J. S. Boyle, R. T. Cederwall, G. L. Potter, and W. Lin (2004), Impact of a revised convective triggering mechanism on Community Atmosphere Model, Version 2, simulations: Results from short-range weather forecasts, *J. Geophys. Res.*, *109*, D14102, doi:10.1029/2004JD004692.

[1]Atmospheric Science Division, Lawrence Livermore National Laboratory, Livermore, California, USA.

[2]Marine Sciences Research Center, State University of New York at Stony Brook, Stony Brook, New York, USA.

0148-0227/04/2004JD004692$09.00

1. Introduction

[2] Convection over land is overactive during the warm season in the National Center for Atmospheric Research (NCAR) Community Atmosphere Model, Version 2 (CAM2), and its previous version (Community Climate Model, Version 3 (CCM3)). This has been found in its single-column model (SCM) simulations [*Xie and Zhang*,

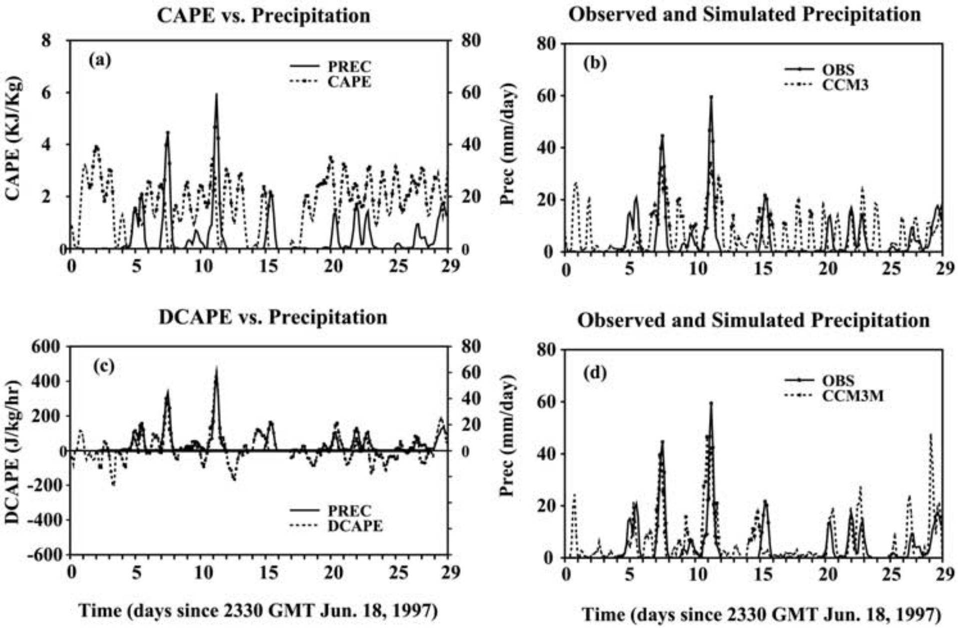

Figure 1. (a) Relationship between CAPE (dotted line) and surface precipitation in the ARM observations during the summer 1997 SGP IOP. (b) Observed (solid line) and CCM3 SCM-produced (dotted line) surface precipitation rates (mm d^{-1}). (c) Relationship between DCAPE and surface precipitation in the ARM observations during the summer 1997 SGP IOP. (d) Observed surface precipitation rates (mm d^{-1}) (solid line) and those produced by the CCM3 SCM with an improved convective trigger (dotted line).

2000; *Ghan et al.*, 2000; *Xie et al.*, 2002; *Zhang*, 2002], full general circulation model (GCM) short-range weather forecasts (J. S. Boyle et al., Diagnosis of CAM2 in NWP configuration, submitted to *Journal of Geophysical Research*, 2004) (hereinafter referred to as Boyle et al., submitted manuscript, 2004), and climate simulations [*Dai and Trenberth*, 2004]. These studies showed that the model (CAM2 or CCM3) tended to produce convective precipitation almost every day during the summer daytime. They found that this problem is closely related to the convection triggering mechanism used in its deep convection scheme [*Zhang and McFarlane*, 1995] (hereinafter referred to as ZM), which assumes that convection is triggered whenever there is positive convective available potential energy (CAPE) (note that CAPE larger than 75 J kg^{-1} is required when the ZM scheme was implemented in CAM2). The positive CAPE triggering mechanism prevents conditional instability from accumulating in the model before convection begins. As a result, it initiates model convection too often during the day because CAPE is almost always positive during the day because of solar heating and the induced CAPE diurnal change over land in the warm season.

[3] To illustrate this problem, Figure 1a shows the time series of CAPE (dotted line) and surface precipitation (solid line) from the observations of the Atmospheric Radiation Measurement (ARM) Program [*Stokes and Schwartz*, 1994; *Ackerman and Stokes*, 2003] 1997 summer Intensive Operational Period (IOP) at its Southern Great Plains (SGP) site. This IOP covers a period from 2330 geomagnetic time (GMT) 18 June to 2330 GMT 17 July 1997. CAPE is calculated from the ARM balloon soundings under the assumption that an air parcel ascends along a reversible moist adiabat with the level of origin at the surface (see equation (2) in section 2). It is clear that the ARM SGP site experienced several intensive precipitation events and dry and clear days during this IOP. Most of the convective events occurred in late evening and early morning. Here local noon (standard time) corresponds to 1800 GMT. The observed CAPE, however, exhibits a strong diurnal variation, with a maximum during the day and a minimum during the night resulting from the strong solar diurnal cycle during summer. On the basis of the positive CAPE trigger, therefore, it is not surprising to see that the CCM3 SCM produced convective precipitation almost every day during the daytime in this IOP (Figure 1b), where the CCM3 SCM is driven by the large-scale dynamical forcing derived from sounding data collected from this ARM IOP using a constrained variational analysis technique [*Zhang and Lin*, 1997; *Zhang et al.*, 2001].

[4] Observations over both midlatitude lands and tropical oceans show that CAPE usually accumulates before convection occurs [e.g., *Zhang and McFarlane*, 1991; *Wang and Randall*, 1994]. The accumulation of large reservoirs of CAPE in nature is a prerequisite for strong convection. To prevent CAPE from being released spontaneously, many efforts have been made in the past to link convective trigger to the large-scale dynamic processes (e.g., large-scale low-level convergence) since these processes play a key role in destabilizing the atmospheric structure and initiating deep cumulus convection. For example, *Kuo* [1965, 1974] linked the convective trigger with the large-scale moisture convergence in his convection scheme. *Fritsch and Chappell* [1980], *Kain and Fritsch* [1993], and *Rogers and Fritsch* [1996] parameterized perturbations of temperature and vertical velocity on the basis of the large-scale low-level

convergence to help avoid excessive convection in areas where the low-level upward motion is weak. To reduce the problem associated with the convective triggering mechanism in the ZM scheme, *Xie and Zhang* [2000] introduced an empirical dynamic constraint after experimenting with a variety of potential large-scale control variables. A dynamic CAPE generation rate (DCAPE) determined by the large-scale advective tendencies of both the temperature and moisture is used to control the onset of deep convection. In their study, DCAPE is defined as the change of CAPE solely due to the total large-scale advection over a time interval (see equation (1) in section 2). They assumed that deep convection occurs only when the large-scale advection makes a positive contribution to the existing positive CAPE. This large-scale dynamic constraint allows CAPE to accumulate from surface processes before convection occurs, and it also links model deep convection closely to the large-scale dynamical processes, including large-scale upward motion and low-level moisture convergence. *Xie* [1998] showed a strong in-phase correlation between positive DCAPE and convective activities using data collected over both midlatitude land and tropical ocean. This relationship is also shown in this 1997 summer ARM IOP data (Figure 1c). Using the CCM3 SCM, *Xie and Zhang* [2000] showed that the dynamic constraint could largely reduce the effect of the strong diurnal variation in the surface insolation on the initiation of convection and that considerable improvements can be obtained in the model simulation of precipitation field when the dynamic constraint was applied to the model triggering function (Figure 1d). However, the performance of the improved convection triggering mechanism in the full GCM has not been tested. In addition, the ARM SGP site is very unique in that warm season moist convection occurs mostly at night rather than in the afternoon as is the case for most other land areas [*Dai*, 2001]. How the revised trigger function works in other areas needs to be examined.

[5] We recently implemented the convection triggering mechanism proposed by *Xie and Zhang* [2000] in the CAM2 model and evaluated its impact on CAM2 simulations in both short-range weather forecasts and climate simulations. The short-range weather forecasts are conducted under the U.S. Department of Energy (DOE)'s Climate Change Prediction Program (CCPP)-ARM Parameterization Testbed (CAPT) framework [*Phillips et al.*, 2004], which provides a flexible environment for running climate models in numerical weather prediction (NWP) mode. In comparison with testing physical parameterizations in climate simulations, the CAPT strategy uses more available observations and high-frequency NWP analyses to evaluate model performance in short-range weather forecasts. This allows specific parameterization deficiencies to be identified before the compensation of multiple errors masks the deficiencies, as can occur in model climate simulation. Another advantage of the CAPT approach is its capability to link model deficiencies directly with atmospheric processes through case studies using data collected from major field programs (e.g., ARM). In this paper, we will focus on evaluating model performance from the CAPT framework. The impact of the new triggering mechanism on climate simulations will be reported in a separate study.

[6] This paper is organized as follows. Section 2 briefly describes CAM2 and model initialization procedures. Section 3 discusses comparison strategy and evaluation data. Comparison of model results with the ARM observations during the 1997 summer IOP at the ARM SGP site is discussed in section 4. Section 5 provides regional and global views on the model performance by comparing with satellite measurements and NWP reanalysis data. Results are summarized in section 6.

2. CAM2 and Model Initialization Procedures

[7] The model used in this study is the NCAR Community Atmosphere Model, Version 2 (CAM2) [*Collins et al.*, 2003] (available online from http://www.ccsm.ucar.edu/models/atm-cam/docs/), which is the fifth generation of the NCAR atmospheric GCM. It is a global spectral model with T42 truncation ($2.8^\circ \times 2.8^\circ$, which is around 300 km) in the horizontal and 26 levels in the vertical. Compared to its earlier version, CCM3 [*Kiehl et al.*, 1998], CAM2 incorporates significant improvements to its physical parameterizations, including generalized cloud overlap for radiation calculation, a new parameterization for longwave absorptivity and emissivity of water vapor, a prognostic scheme for cloud condensed water, a new sea ice formulation, an explicit representation of fractional land and sea ice coverage, and evaporation of convective precipitation. CAM2 retains the same deep convection scheme (the ZM scheme) as used in CCM3. The ZM scheme is based on the plume ensemble concept, similar to that of *Arakawa and Schubert* [1974]. Shallow convection is represented using the scheme developed by *Hack* [1994]. More detailed information about CAM2 is given by *Collins et al.* [2003].

[8] As discussed earlier, the ZM scheme assumes that convection occurs whenever there is a positive CAPE. In reality, convection is triggered when an air parcel or a subgrid-scale cell is sufficiently perturbed to penetrate the layer of convection inhibition. This penetration is typically associated with one of the following scenarios: large-scale upward motion associated with synoptic-scale systems, existing convection, subgrid-scale dynamic instability, surface heterogeneity, or growth of the boundary layer. After experimenting different control variables observed at the ARM SGP site, *Xie and Zhang* [2000] (hereinafter referred to as XZ trigger) found that the large-scale dynamic condition had the dominant control on the occurrence of convection and that the combined measure of lifting and inhibition was empirically described by the positive contribution of large-scale advection to CAPE, including upward motion and lower level moistening by the grid-scale circulation. The role of large-scale forcing in controlling convection over the central United States (which often occurs at night) was also given by *Dai et al.* [1999], in which the nocturnal convection has been linked to diurnal variations of low-level convergence resulting from surface pressure tides. In this study, we implement the XZ trigger in the CAM2. It requires that deep convection occur only when the large-scale advective tendencies of temperature and moisture make a positive contribution to the existing

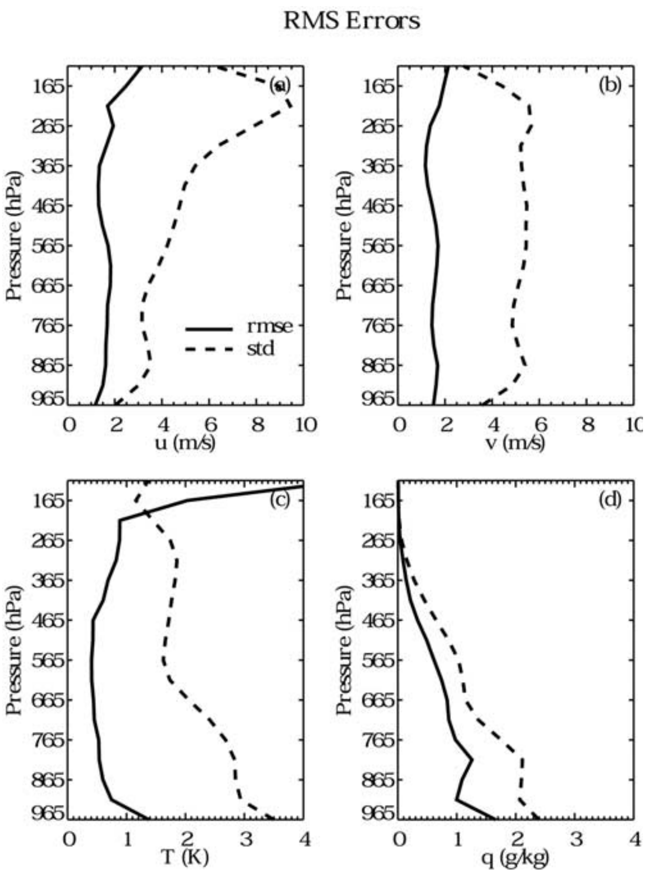

Figure 2. RMS errors (solid lines) in the ERA-40 reanalyses of (a) horizontal wind u component, (b) v component, (c) temperature, and (d) moisture during the ARM summer 1997 IOP. Dashed lines represent standard deviations of the ARM observed fields.

positive CAPE, i.e., DCAPE > 0 and CAPE > 0, in which DCAPE is defined as

$$\mathrm{DCAPE} = [\mathrm{CAPE}(T^*,\ q^*) - \mathrm{CAPE}(T, q)]/\Delta t, \tag{1}$$

where (T, q) are the temperature and specific humidity in the current atmospheric state and (T^*, q^*) are (T, q) plus the changes due to the total large-scale advection over a time interval Δt, which is equal to the time step used in CAM2. These changes can be obtained by taking the differences in (T, q) just before and after the calculation of model dynamics in CAM2. CAPE is calculated under the assumption that an air parcel ascends along a reversible moist adiabat.

$$\mathrm{CAPE} = R_d \int_{P_i}^{P_n} \left(T_{vp} - T_v\right) \mathrm{d}\ \ln p, \tag{2}$$

where P_n is the neutral buoyancy pressure for an air parcel originating from P_i. T_{vp} is the virtual temperature of the parcel, and T_v is the virtual temperature of the ambient air at the same level.

[9] As part of the CAPT framework, the CAM2 model is initialized with the European Centre for Medium-Range Weather Forecasts (ECMWF) reanalysis (ERA-40) (ECMWF re-analysis ERA, 2002, accessible online at http://www.ecmwf.int/research/era). The ERA-40 reanalysis data were generated every 6 hours by implementing a three-dimensional variational analysis technique that uses the T159L60 version of the ECMWF Integrated Forecasting System. In our implementation, the dynamical atmospheric variables were interpolated from the finer-resolution reanalysis grid to the CAM2 grid using the procedures described by *White* [2001] (also accessible online at http://www.ecmwf.int/research/ifsdocs_old/TECHNICAL/index.html). These procedures use a slightly different interpolation approach for each of the dynamic state variables, u, v, T, q, and P_s, along with careful adjustments to account for the difference in representation of the Earth's topography between the reanalysis and CAM2 models. Initial values for the prognostic parameterized variables (e.g., cloud water) are obtained via a spin-up procedure in conjunction with the land initialization. There are three steps used to initialize the land for CAM2: (1) Produce a climatological seasonal land data set by running CAM2 for many years using climatological SSTs. (2) Run CAM2 in a nudging mode starting from the climatology generated in step 1 for a sufficient time. (3) Run CAM2 in a forecast/analysis mode for a short period preceding the time of interest to fine-tune the land, at least in the upper layers. In the nudging mode the predicted atmospheric state variables are nudged toward the reanalysis at a specified timescale (i.e., 6 hours). In the forecast/analysis mode the atmospheric variables are periodically updated (i.e., 6 hours) with the interpolated analyses, and the coupled land/atmosphere system is allowed to evolve until the next update time. Details about the initialization procedures are given by *Phillips et al.* [2004].

[10] To examine the quality of the initial data, Figure 2 gives the root-mean-square (RMS) errors (solid lines) of the atmospheric state variables from the ERA-40 reanalysis averaged over the ARM SGP domain for the 1997 summer IOP. The standard deviations of the ARM observed fields (dashed lines) are also shown in the figure to show the size of the RMS error relative to the variability in the observed field itself. The RMS error in the ERA-40 reanalysis is typically less than 1.5 m s^{-1} in the horizontal winds within most of the troposphere except the levels above 315 hPa, where the RMS error is slightly larger. The temperature field shows an RMS error of around 0.5 K in the middle and lower troposphere between 865 hPa and 465 hPa and less than 1 K for the entire troposphere from 915 hPa to 215 hPa. Near the surface and above 215 hPa, the temperature error is quite large. The RMS error in the moisture field decreases with height. It is less than or around 1 g kg^{-1} in most of the troposphere except for the lowest level, where the RMS error is $\sim$1.5 g kg^{-1}. These errors may in part occur because the ARM sounding measurements were not used in the ERA-40 data assimilation system. The rather large errors shown in horizontal winds and temperature in the upper troposphere may be also due to relatively large uncertainties in the ARM sounding measurements at those levels. In comparison with the observed standard deviations (dashed lines), the RMS

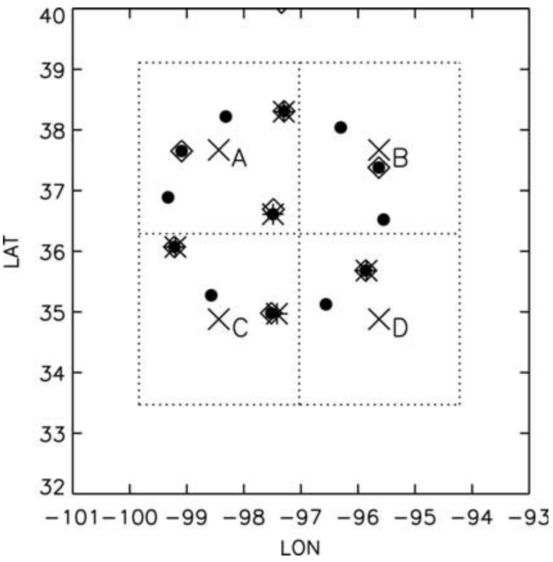

Figure 3. Locations of the ARM five sounding balloons (stars), the seven NOAA wind profilers (open diamonds), the CAM2 model grids (crosses), and the variational analysis domain (solid circles) at the ARM SGP site. The letters A, B, C, and D represent the four CAM2 grid boxes centered by the model grid points (crosses), respectively.

errors are considerably smaller than the observed temporal variability itself.

3. Comparison Strategy and Evaluation Data

[11] To evaluate model physical parameterizations, a series of short-range forecasts (24 hours) were conducted under the CAPT framework in order to ensure that the model-produced large-scale circulation has not been drifted away from observations. These runs were initiated every day at 0000 UT for 30 days starting from 18 June 1997 to 17 July 1997 to cover the ARM 1997 summer IOP. We also conducted a sequence of 24-hour forecasts initiated every 6 hours from 18 June 1997 to 17 July 1997 to examine the impact of model spin-up. The difference for the ARM SGP site between the forecasts initialized at different times of the day is much less significant than the main features presented in this work. Therefore, in the following discussions, we will focus our analysis on results from the series of 24-hour forecasts initiated every day at 0000 UT. Selected meteorological fields are discussed with a focus on the model-simulated precipitation and other associated fields. Comparisons are made with both field measurements and global satellite data and NWP reanalyses.

[12] The field measurements are from the data collected from the ARM SGP site during its 1997 summer IOP, which contained a wide range of summertime midlatitude weather conditions. The ARM Program is a key part of the DOE effort to address scientific uncertainties in global climate changes with a specific focus on improving the performance of current climate models for climate research and prediction. To reach this goal, the ARM Program has conducted a number of extensive field campaigns to collect data for evaluation and improvement of model physical parameterizations, especially radiation and cloud parameterizations. During the ARM IOPs, sounding balloons at five sounding stations (stars in Figure 3) are launched every 3 hours to measure the vertical profiles of temperature, water vapor mixing ratio, and winds. There are also seven National Oceanic and Atmospheric Administration (NOAA) wind profiler stations near the SGP site (open diamonds in Figure 3) taking hourly winds. Within the SGP domain (circled by the variational analysis grids (solid circles) in Figure 3) there is a dense surface measurement network, which was described by *Zhang et al.* [2001], along with satellite measurements from the Geostationary Operational Environmental Satellite (GOES). These platforms include the Surface Meteorological Observation System (SMOS) and the Oklahoma and Kansas mesonet (OKM and KAM) stations, which measure surface precipitation, pressure, winds, temperature, and relative humidity; the energy balance Bowen ratio (EBBR) stations and the eddy correlation flux measurement system (ECOR), which measure surface latent and sensible heat fluxes and surface broadband net radiative flux; the microwave radiometer (MWR) stations, which measure the column precipitable water and total cloud liquid water; and the surface Solar Infrared Radiation Stations (SIRS), which provide 1-min continuous measurements of broadband shortwave and longwave irradiances for downwelling and upwelling components. The hourly Arkansas-Red Basin River Forecast Center (ABRFC) 4-km rain gauge adjusted WSR-88D radar measurements over the domain are also available and provide the best estimate of the spatial distribution of precipitation. The satellite measurements of clouds and broadband radiative fluxes are available from the $0.5^\circ \times 0.5^\circ$ analysis of the GOES data [*Minnis et al.*, 1995].

[13] To make comparisons more meaningful between model outputs and the ARM observations, the SGP domain-averaged ARM data are needed. The domain-averaged atmospheric state variables are obtained from merging the sounding and wind profiler data through the constrained objective variational analysis [*Zhang and Lin*, 1997; *Zhang et al.*, 2001]. In order to avoid biases of using overcrowding measurement stations in some areas, the domain-averaged surface variables are obtained by first laying the $0.5^\circ \times 0.5^\circ$ GOES grids over the SGP domain and then deriving the required quantities in each small grid box. If there are actual measurements within the subgrid box, simple arithmetic averaging is used to obtain the subgrid means. Some variables are available from several instruments as discussed earlier. They are merged in the arithmetic averaging process. If there is no actual measurement available in the small box, the Barnes scheme [*Barnes*, 1964] is used to fill the missing data. Domain averages of these quantities are obtained by using values from the $0.5^\circ \times 0.5^\circ$ grid boxes within the analysis domain. More details are given by *Zhang et al.* [2001].

[14] Since the CAM2 grid box does not match the SGP domain exactly, as shown in Figure 3, which gives four surrounding model grid boxes (the four small squares A, B, C, and D centered by the model grid points (crosses)) at the ARM SGP site, model outputs are averaged over the four model grid boxes using weights proportional to the overlap area of the CAM2 grid box with the ARM SGP domain when compared with the ARM observations. Therefore model results actually represent averages over a domain that is slightly larger than the ARM SGP domain. This should be borne in mind in the following discussions.

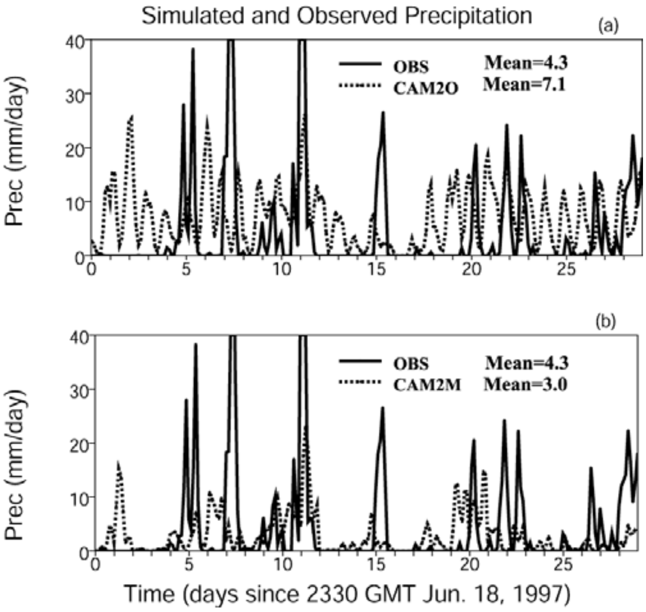

Figure 4. Time series of the observed (solid lines) and model-simulated (dotted lines) surface precipitation rates (mm d^{-1}) during the ARM 1997 summer IOP. (a) CAM2O versus OBS. (b) CAM2M versus OBS. The mean precipitation rates over this IOP from the observations and the models are also shown in the figure.

[15] As discussed earlier, the ARM SGP site is different from most land areas in that it has a nocturnal maximum of moist convection in the warm season instead of an afternoon maximum elsewhere [*Dai*, 2001]. Therefore it is necessary to evaluate model results in the areas beyond the ARM SGP site. For this purpose, we compare the model-produced precipitation with the observations taken from Global Precipitation Climatology Project (GPCP) daily 1° × 1° gridded precipitation data [*Huffman et al.*, 2001]. The GPCP precipitation data are obtained by merging satellite estimates of precipitation with rain gauge data from surface-based stations. The model clouds are evaluated against the measurements from International Satellite Cloud Climatology Project (ISCCP) D1 3-hourly cloud products [*Rossow et al.* 1996]. ISCCP cloud products classify cloud types on the basis of their top pressure and optical thickness. To facilitate the evaluation, an ISCCP simulator [*Klein and Jakob*, 1999; *Webb et al.*, 2001] is added as a run time diagnostic package in CAM2 to emulate the ISCCP algorithm. The ISCCP simulator diagnoses model clouds in a similar the way that a satellite would view an atmosphere with physical properties (e.g., cloud height, cloud cover, and optical depth) specified by the model. *Lin and Zhang* [2004] described the details of implementing the ISCCP simulator in CAM2. For the atmospheric state variables we compare the model simulations with the ERA-40 reanalyses.

4. Comparison With the ARM Measurements at the SGP Site

4.1. Time Series of Precipitation, Clouds, and Surface Temperature

[16] We first examine the model-produced surface precipitation rates since they are closely associated with the model cumulus convection scheme. For convenience, we use CAM2O to represent the original model, CAM2M to represent the model with the modified triggering mechanism, and OBS to represent observations in the following discussions. Figure 4 shows the time series of surface precipitation rates for CAM2O, CAM2M, and the corresponding observations averaged over the ARM SGP domain. The model result is 0- to 24-hour forecasts from a series of 24-hour runs concatenated for the ARM 1997 summer IOP. We use the same method to construct other fields. As we discussed in section 1, during this IOP, the ARM SGP site experienced several intensive precipitation events and dry and clear days. Most of the heavy precipitation events are associated with a complex of thunderstorms that developed outside the ARM SGP domain in the late evening and moved across the ARM SGP domain (e.g., the precipitation events on days 8, 11–12, and 21). Here "day n" refers to the day between $n - 1$ and n in the plots. This convention is used throughout the paper. Some precipitation events are associated with localized individual thunderstorms (e.g., the weak precipitation event on day 10 and the moderate precipitation events on days 22–23). Most of the convective events produced cumulus precipitation [*Xie et al.*, 2002]. The dry and clear periods are associated with strong large-scale downward motions.

[17] It is seen that the original CAM2 greatly overestimates the frequency of the observed precipitation occurrence. It tends to produce precipitation almost every day (Figure 4a), similar to the results seen in the CCM3 SCM test (Figure 1b). This is also a major problem in CAM2 climate simulation as documented by *Dai and Trenberth* [2004]. This problem is noticeably reduced in CAM2M when the XZ trigger is used (Figure 4b). The dynamic constraint introduced in the XZ trigger effectively prevents convection from being fired every day in the model. We also notice that the observed mean precipitation rates (4.3 mm d^{-1}) over the entire period are substantially overestimated by CAM2O (7.1 mm d^{-1}) because of the overestimation of the rain frequency. In contrast, the observed value is underestimated by CAM2M (3.0 mm d^{-1}), which is related to the fact that CAM2M misses or considerably underestimates a number of strong convective events (e.g., on days 5, 7–8, and 15–16) during the period. This is partially associated with errors in the model-produced large-scale dynamical fields (e.g., vertical motion and advection terms), which are directly related to the DCAPE used in the XZ convective trigger function. Note that the large-scale dynamical processes and the model physical processes interact with each other in the GCM and uncertainties in the model parameterizations can have large impacts on the model-produced large-scale dynamical fields [*Xie et al.*, 2003]. Figure 5 compares the observed and model-produced vertical velocity (omega) field for the first 16 days, which cover several strong convective events. The observed surface precipitation rates are also shown in Figure 5a. It is seen that the model-produced upward motions (Figures 5b and 5c) are considerably weaker than the ARM observed values (Figure 5a) during these strong convective events (e.g., days 5, 7–8, 11–12, and 15–16). The weaker forcing results in the weaker precipitation produced by the models. This can also explain why the revised scheme works better in the CCM3 SCM (Figure 1d) than it does in the GCM

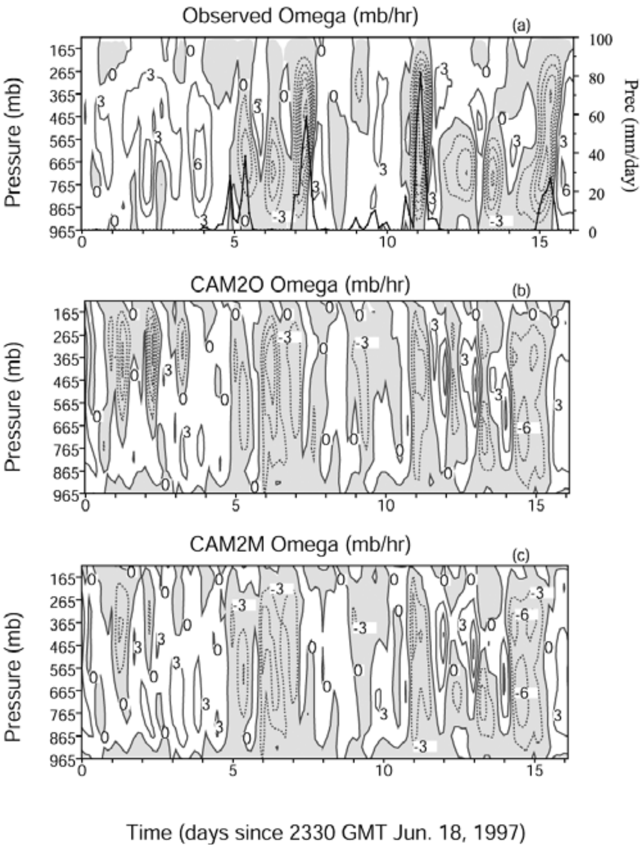

Figure 5. Temporal evolution of the derived vertical velocity (omega) from (a) the ARM observations, (b) CAM2O, and (c) CAM2M for the first 16 days during the ARM 1997 summer IOP. Contour interval is 3. The units in the figure are hPa h^{-1}. Contours less than 0 are shaded. In Figure 5, solid lines are for contours greater than or equal to zero, and dotted lines are for contours less than zero. The thick solid line in Figure 5a is the observed surface precipitation rate (mm d^{-1}).

(Figure 4b) since the forcing in an SCM is specified from the observations.

[18] It should be noted that the underestimation of the observed precipitation events is not uncommon in climate models, which typically use horizontal resolutions that are larger than 200 km, in simulating these subgrid-scale-dominated convective processes. The problem could be reduced by increasing the model resolutions [*Duffy et al.*, 2003]. In addition, the model precipitation is averaged over an area that is slightly larger than the ARM SGP domain (see Figure 3). This could also contribute to the error in both the magnitude and the frequency of the events produced in the models. We checked the radar rainfall estimates over a larger region that matches the four CAM2 grid boxes and found that the rain events do occur more often with slightly reduced magnitudes of the precipitation peaks over the larger region. Nonetheless, CAM2O still significantly overestimates the frequency of the observed rain events, and both CAM2O and CAM2M significantly underestimate the magnitude of these precipitation peaks.

[19] The diurnal variation of the observed and model-produced surface precipitation is shown in Figure 6. The observations show a rather clear diurnal variation in precipitation, with the maximum at 2100 local standard time (LST) and the minimum at 1200 LST. In contrast, CAM2O produces excessive precipitation during the day, with the maximum at 1500 LST and the minimum at 0600 LST. The temporal correlation between the observed and CAM2O produced precipitation is just 0.01. This correlation is increased to 0.2 when the XZ trigger is used. However, CAM2M still shows problems with capturing the observed diurnal cycle correctly. In comparison with the observations, CAM2M shows a rather weak semidiurnal variation in its produced precipitation field. This problem is also partially related to the error in the model-produced large-scale forcing, and it requires further study.

[20] Clouds are another field that is greatly affected by model cumulus parameterizations. Figures 7a and 7b compare the high cloud fraction produced by CAM2O and CAM2M to the GOES satellite observations, respectively. CAM2O shows much larger temporal variability in its produced high clouds in comparison with the GOES high clouds. This is clearly related to the too frequent convection produced in this model. The observed high clouds are overestimated by CAM2O, especially during nonprecipitation periods (e.g., on days 1–4 and days 13–15). The mean high cloud amount over the period is 64.1% in CAM2O in comparison with 26.6% in the observations. In contrast, the observed temporal variability and the mean high cloud amount is well reproduced in CAM2M, and the bias in CAM2O is significantly reduced in CAM2M during non-precipitation periods because of less convection produced with the improved convective trigger. However, it is noticed that Figure 7b shows quite large discrepancies between the observed and CAM2M-produced high clouds on days 2, 5, 7–8, 15–16, 18, and 29. This is related to the biases in the model-produced precipitation field (Figure 4b). Similar results can be seen in the outgoing long-wave radiative flux (OLR, not shown). The OLR simulation is considerably improved in CAM2M, consistent with the improvements in the high clouds.

[21] The observed and model-simulated surface temperature fields are shown in Figure 8. The observations (solid lines) show very strong diurnal variations. This feature is

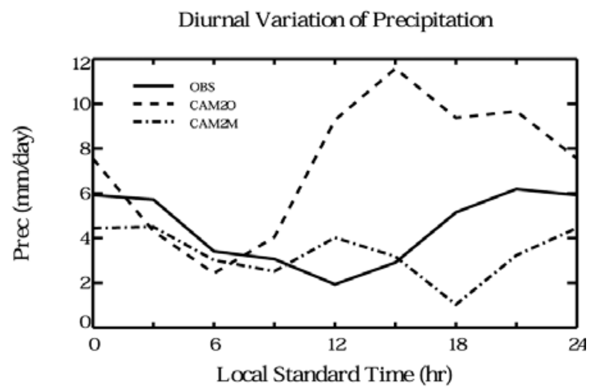

Figure 6. Diurnal variation of surface precipitation in the observations and the models during the ARM 1997 summer IOP.

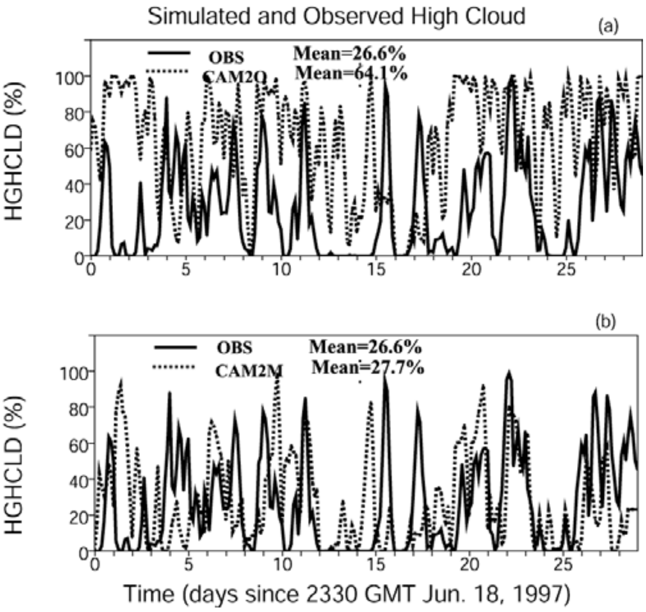

Figure 7. Time series of the observed (solid lines) and model-simulated (dotted lines) high clouds (percent) during the ARM 1997 summer IOP. (a) CAM2O versus OBS. (b) CAM2M versus OBS. The mean high-cloud amount over this IOP from the observations and the models is also shown in the figure.

well captured by both models. However, the surface temperature in CAM2O is too cold (2.4 K colder in terms of the mean surface temperature) compared to the observations (Figure 8a). One of the reasons is because convection is too active in CAM2O, which results in excessive clouds, leading to less solar radiation reaching the surface. With the new triggering scheme the excessive clouds are largely reduced. This leads to large improvements in the surface temperature simulation, especially during the day when surface temperature reaches the maximum (Figure 8b).

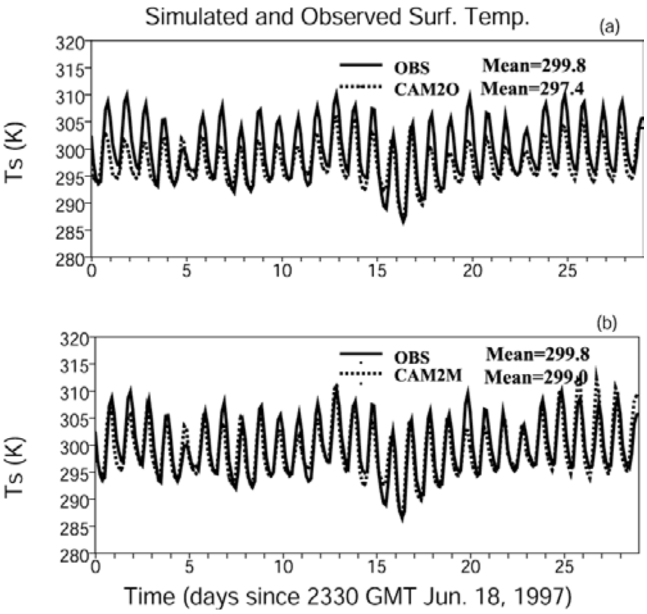

Figure 8. Time series of the observed (solid lines) and model-simulated (dotted lines) surface temperature (K) during the ARM 1997 summer IOP. (a) CAM2O versus OBS. (b) CAM2M versus OBS. The mean surface temperature over this IOP from the observations and the models is also shown in the figure.

4.2. Simulations of Atmospheric Temperature and Moisture Fields

[22] The temporal evolution of the ARM observed temperature and differences between the simulated temperature and the observed value over the SGP domain are shown in Figure 9. The original model (CAM2O) shows a systematic warm bias in most of the troposphere, especially in the middle and upper troposphere between 565 hPa and 215 hPa, when compared to the ARM observations (Figure 9b). The warm bias is clearly related to the model-produced overactive convection, which releases excessive convective heating at these levels. While this error is also shown in

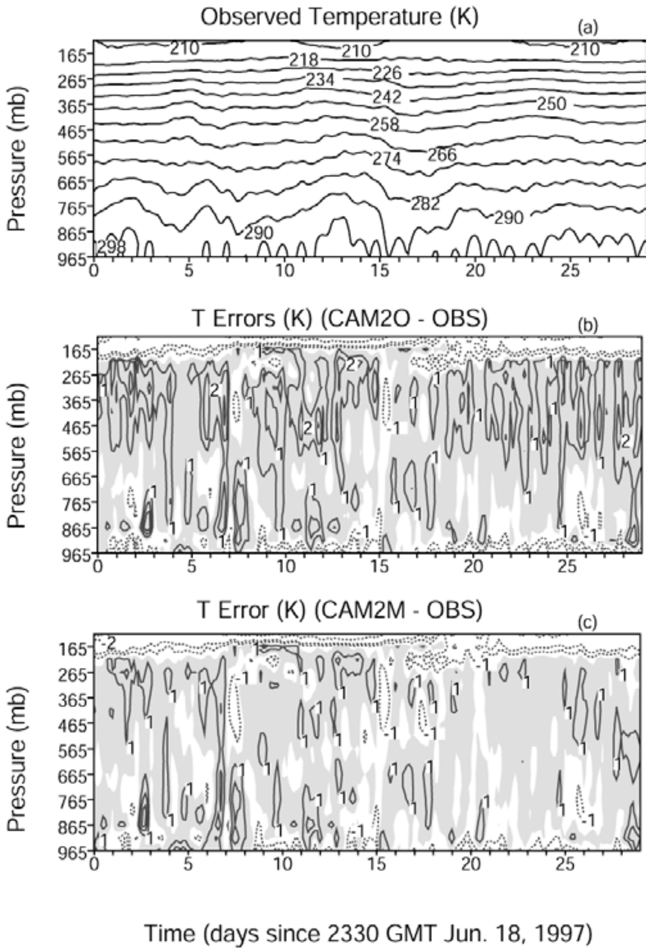

Figure 9. Temporal evolution of (a) the ARM observed temperature, (b) differences between the CAM2O-simulated temperature and the observations, and (c) differences between the CAM2M-simulated temperature and the observations. The units in the panels are K. Contour interval in Figure 9a is 8. In Figures 9b–9c, contours larger than 0 are shaded. Contour interval is 1. Solid lines are for contours greater than or equal to zero, and dotted lines are for contours less than zero.

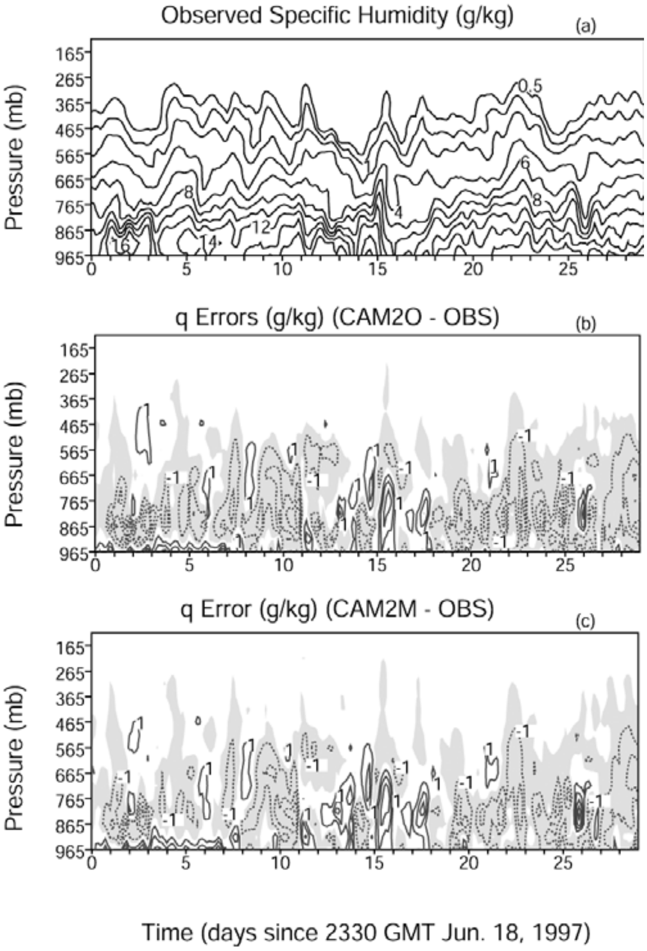

Figure 10. Same as Figure 9 except for the moisture field. The units are g kg^{-1}. Contours in Figure 10a are 0, 0.5, 1.0, 2.0, 4.0, 6.0, 8.0, 10, 12, 14, and 16. In Figures 10b and 10c, contours less than 0 are shaded. Contour interval is 1. Solid lines are for contours greater than or equal to zero, and dotted lines are for contours less than zero.

CAM2M, it has been considerably reduced (Figure 9c). The largest improvement is between 565 hPa and 215 hPa. Beyond these levels, both CAM2O and CAM2M display a very similar error pattern with a comparable magnitude of the model bias. Both models become too cold in the level above 215 hPa. This is probably related to the error in the initial data, which show a rather large cold bias above 215 hPa compared to the ARM data (not shown).

[23] Figure 10 is the same as Figure 9 except for the moisture simulation. Both CAM2O and CAM2M (Figures 10b and 10c) show a systematic dry bias in the middle and lower troposphere over the entire period except for days 16–18, when both models produce a significant moist bias due to the failure to capture the abrupt reduction of moisture shown in the observations during that period (Figure 10a). However, the magnitude of the dry bias in CAM2M is smaller than that in CAM2O because convection is less active in CAM2M than it is in the original model. This results in less moisture consumed by convection in CAM2M.

[24] To show the improvement more clearly, Figures 11a and 11b display the vertical distributions of the RMS errors in temperature and moisture (compared to the ARM data) for the 30 days, respectively. It is seen that CAM2M shows smaller RMS errors for the entire column when compared to CAM2O. The largest improvements are seen in the middle and upper troposphere for temperature and in the lower troposphere for moisture.

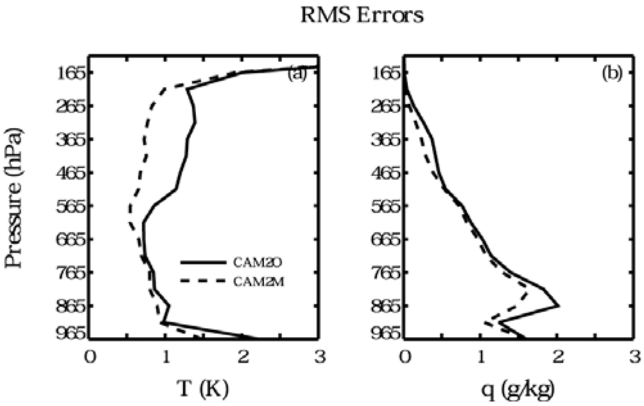

Figure 11. Vertical profiles of the RMS errors in the CAM2O-simulated (solid lines) and CAM2M-simulated (dashed lines) (a) temperature and (b) moisture fields during the ARM 1997 summer IOP.

4.3. Mean Surface Energy Budgets

[25] Table 1 presents the time-averaged surface energy budget components for CAM2O, CAM2M, and the ARM observations over the entire IOP at the SGP site. In the table, SWS and LWS are net surface shortwave and longwave radiative fluxes, respectively. LH is surface latent heat flux, and SH is surface sensible heat flux. The observed surface radiative fluxes are from the ARM surface Solar Infrared Radiation Station measurements. The ARM EBBR and ECOR instruments provide the observed surface latent and sensible heat flux data.

[26] It is seen from the table that the simulated surface net shortwave and longwave radiative fluxes in CAM2O are smaller than observed by −23.5 W m^{-2} for shortwave radiation and −7.5 W m^{-2} for longwave radiation, respectively. CAM2O-simulated sensible heat flux is 25.6 W m^{-2} less than the ARM observations, which is consistent with the colder surface produced in the model (Figure 8a), and latent heat flux is 32.4 W m^{-2} larger than the observed. For these surface energy budget terms, CAM2M shows much better agreement with the observations than does CAM2O. The differences between CAM2M and the observations are

Table 1. Mean Surface Energy Budgets Averaged Over the ARM 1997 Summer IOP for the SGP Site[a]

Field	Observation	CAM2O	CAM2M
SWS	227.483	203.944	221.878
LWS	63.409	55.938	63.979
LH	113.640	146.049	131.583
SH	36.279	10.714	27.435
Net surface	14.567	−8.757	−1.119

[a]Mean surface energy budgets are given in W m^{-2}.

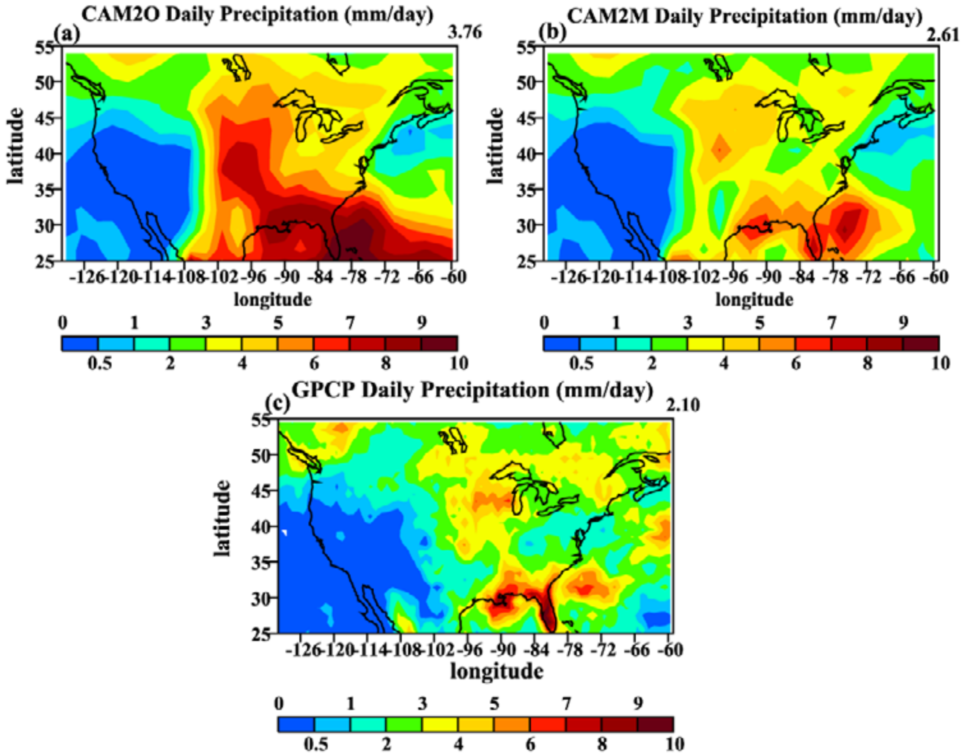

Figure 12. Geographical distribution of a 30-day mean precipitation of 0–24-hour forecasts over the continental United States for (a) CAM2O, (b) CAM2M, and (c) the GPCP data, respectively. The regional mean precipitation rates (mm d^{-1}) are shown at the top right of the panels.

within 6 W m^{-2} in shortwave radiation, 0.5 W m^{-2} in longwave radiation, 8.8 W m^{-2} in sensible heat flux, and 17.9 in latent heat flux. The net surface energy budget in CAM2M is also much closer to the observed value than that in CAM2O. This is consistent with the more realistic surface temperature produced in CAM2M (Figure 8b).

[27] The above discussions have shown that the XZ trigger improves overall the CAM2 simulations in the short-range weather forecasts when compared to the ARM field measurements. The improvements are similar to those obtained in the SCM tests [e.g., *Xie and Zhang*, 2000]. However, it should be noted that improvements made in SCM tests are not guaranteed to be transferable to its parent GCM because of the limitations of the SCM framework, such as the lack of internal feedback between the model dynamical processes and physical processes. The encouraging results shown in this study indicate that the improved scheme proposed by *Xie and Zhang* [2000] based on the SCM framework has passed the test in a full GCM, at least for the same geographical location (the SGP site).

5. Regional and Global Comparisons

5.1. Precipitation

[28] To examine the impact of the convective triggers on simulations in regions beyond the ARM SGP site, Figure 12 displays the geographical distribution of precipitation over the region that covers the continental United States. The model data are 0–24-hour forecasts averaged over the 30 days as described in section 3. The observations are taken from Global Precipitation Climatology Project (GPCP) daily precipitation data [*Huffman et al.*, 2001], and these data are averaged over the same period as that covered by the model data. During the summer period the heaviest precipitation is seen in the southeast and along the Gulf Coast in the GPCP data (Figure 12c). Another relatively large rainfall region in the observations is located southwest of the Great Lakes along the Mississippi-Wisconsin Rivers. Light precipitation is seen between these two major precipitation areas from the southwestern United States stretching northeastward to the northeast coast. Overall, the observed spatial pattern of precipitation appears to be more realistically simulated in CAM2M than it is in CAM2O (Figures 12a and 12b). The locations of the two maximum precipitation centers in the southeast and along the Gulf Coast in the observations are well captured by CAM2M. Another observed large precipitation region along the Mississippi-Wisconsin Rivers is also reasonably reproduced in CAM2M, although the area of the modeled precipitation is larger than that of the observations. In contrast, the original model CAM2O overestimates the observed precipitation in most parts of the country. For the regional mean precipitation rate (the numbers at the top right of Figures 12a–12c), CAM2O shows a much larger value (3.76 mm d^{-1}) than the observations (2.10 mm d^{-1}), while the overestimation is considerably reduced in CAM2M (2.61 mm d^{-1}).

[29] It is noticed that CAM2O shows a precipitation maximum located to the east of the Rockies, which is not shown in the observations. This phenomenon is also present in the summer precipitation field for the mean of all Coupled Model Intercomparison Project (CMIP) models

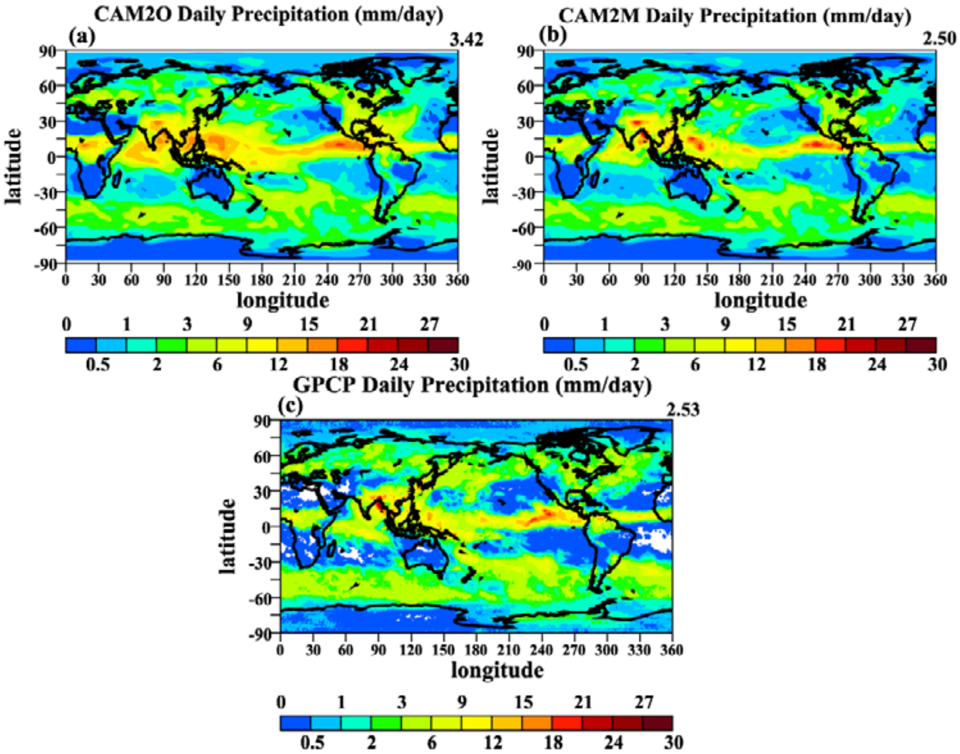

Figure 13. Global distribution of a 30-day mean precipitation of 0–24-hour forecasts for (a) CAM2O, (b) CAM2M, and (c) the GPCP data, respectively. The global mean precipitation rates (mm d^{-1}) are shown at the top right of the panels.

[*Coquard et al.*, 2004]. Results from our study indicate that the CMIP model systematic error can be detected in the early stage of model integration. This has important implications for understanding what model deficiencies cause the systematic error since it allows us to perform a more in-depth analysis during a short time period where more observations are available and different model errors from various processes have not compensated for the systematic error. It is interesting to see that this bias is largely reduced in CAM2M, indicating that problems associated with model cumulus parameterization should partly account for this systematic climate error.

[30] In addition to these improvements over the midlatitude lands, CAM2M also shows very encouraging results in other areas, including the tropical and subtropical regions as shown in Figure 13, which gives the global distribution of precipitation for CAM2O, CAM2M, and the observations. It is seen from Figure 13b that CAM2M reproduces well the principal features of the observed precipitation distribution, particularly in the tropical Pacific and Indian Oceans and in North Africa. In contrast, CAM2O produces excessive precipitation over a broader region in comparison with the observations, but it underestimates the magnitude of the observed precipitation maxima, such as those in the eastern Pacific and at the northeastern boundary of the Bay of Bengal (Figure 13a). Compared to the observed global mean precipitation rate (2.53 mm d^{-1}), CAM2O overestimates the observations by 0.89 mm d^{-1} while CAM2M just slightly underestimates the observations by 0.03 mm d^{-1}. These results indicate that the triggering mechanism developed by *Xie and Zhang* [2000] based on the midlatitude observations is suitable for use globally.

5.2. Clouds

[31] The global distribution of high clouds from CAM2O, CAM2M, and the ISCCP satellite measurements is shown in Figure 14. As discussed earlier, the model clouds are diagnosed by using the ISCCP simulator with cloud physical properties specified from the CAM2 model. Since ISCCP clouds are not available during nighttime, only daytime model clouds from the series of 0–24-hour forecasts are averaged over the 30 days. During the summer period the ISCCP clouds (Figure 14c) show a maximum band of clouds along the equatorial Pacific in the vicinity of the Intertropical Convergence Zone (ITCZ), the southern Asia continents, and Indian Oceans and two minimum bands of clouds in the subtropical regions associated with the strong downward branch of the Hadley circulation. In general, both models capture this spatial pattern of the ISCCP high clouds. However, CAM2O substantially overestimates the high cloud amount in the tropics and underestimates the high clouds in the subtropics and most land areas. Note that these biases are also shown in its climate simulations [*Lin and Zhang*, 2004], indicating that the systematical errors in both climate simulation and weather forecasts could be due to the same deficiencies in the model. In contrast, CAM2M reproduces the observed high clouds remarkably well in the tropics even though it also underestimates the subtropical high clouds as shown in CAM2O. The improvements in the high clouds are consistent with the improvements in the simulated precipitation in the tropical

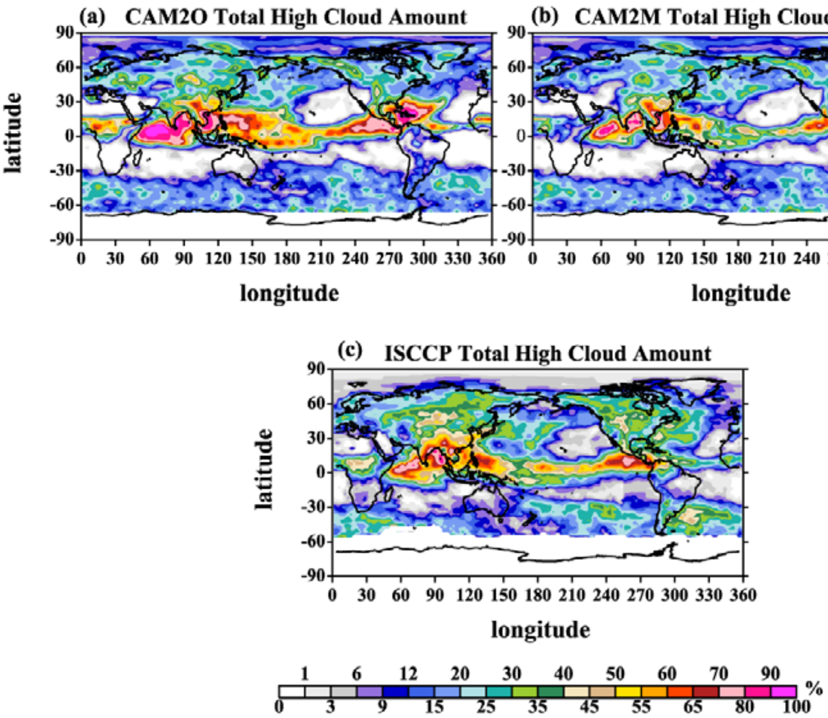

Figure 14. Global distribution of 30-day mean high clouds (daytime only) of 0–24-hour forecasts for (a) CAM2O, (b) CAM2M, and (c) the ISCCP data, respectively.

regions and most land areas as shown in Figure 13. The result suggests that the systematic overestimation of the observed high clouds in the tropics in CAM2 may be largely related to problems associated with its deep convection scheme rather than its cloud scheme.

5.3. Temperature, Moisture, and Zonal Wind

[32] The model-produced zonally averaged mean temperature, moisture, and zonal wind from the series of 24-hour forecasts over the 30 days are compared with the ERA-40 reanalysis data. Figures 15a–15c give the zonally averaged mean temperature from the ERA-40 reanalyses and the differences between the models and the reanalysis data, respectively. In comparison with the reanalysis data, both models produce very similar errors in the lower and upper troposphere, such as the quite large warm biases in the midldle and high latitudes in both hemispheres below 800 hPa. Between 600 hPa and 200 hPa the temperature error produced by CAM2O and CAM2M is quite different, especially in the tropical and subtropical regions from 30°N to 30°S, where CAM2O shows a rather large warm bias of up to 1 K while CAM2M just produces a small cold bias (less than −0.5 K). The warm bias in CAM2O is likely related to its overestimation of convection in these regions as indicated in its precipitation field (Figure 13a). In general, CAM2M produces a colder atmosphere with smaller errors than CAM2O in the midtroposphere and a rather large cold tropical bias between 700 and 800 hPa because of less convection triggered in the model and also likely the interaction of convection with other model physics.

[33] Similar results are also seen in the zonally averaged mean moisture field (Figures 16a–16c). Compared to the ERA-40 reanalyses, the model error in moisture field is small in the middle and high latitudes because there is less moisture in these regions than in the tropical and subtropical regions (Figure 16a). Between 30°N and 30°S, CAM2O produces a large dry bias in the lower troposphere (Figure 16b), which is consistent with the large warm bias shown in the middle and upper troposphere in its temperature simulation (Figure 15b). Again, this indicates that convection in CAM2O is too active, which results in excessive moisture consumed in the lower troposphere and excessive convective heating released in the midtroposphere and upper troposphere. With the new convective trigger, CAM2M dramatically reduces this dry bias (Figure 16c). It is also noted that both models show a relatively large moist bias near the surface. This may reflect problems associated with model boundary layer processes, which are not able to effectively transport moisture from the surface to the upper troposphere. As shown by Boyle et al. (submitted manuscript, 2004), the boundary height produced by the CAM2 model is too low compared to the ARM measurements at the SGP site.

[34] The zonal wind is another important field that people usually use for verification of model simulation. During the summer season the ERA-40 reanalysis data show a strong westerly maximum at 200 hPa near 40°N over the North Hemisphere and a stronger westerly maximum at 200 hPa near 30°S over the Southern Hemisphere (Figure 17a). In the tropical regions, the ERA-40 reanalyses show weak easterlies. Overall, the zonal wind structure is well simulated by both models. However, the zonally averaged westerlies in CAM2O are much stronger than the reanalysis data in the upper troposphere between 30°N and 40°N and between 10°S and 30°S (Figure 17b). This is probably

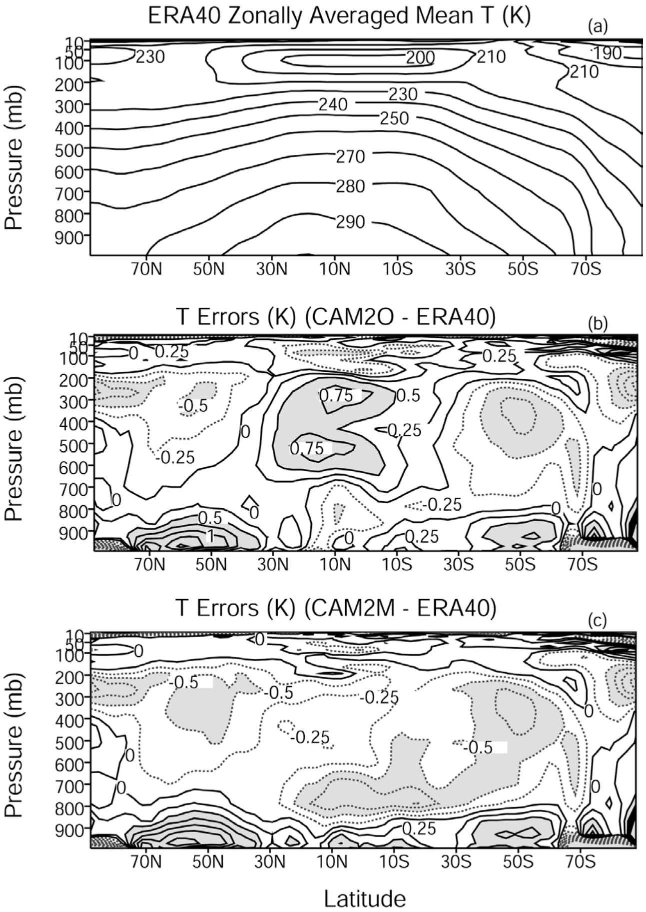

Figure 15. (a) Zonally averaged mean temperature over the 30 days from ERA-40 and the differences (b) between CAM2O and ERA-40 and (c) between CAM2M and ERA-40. Units are K. In Figures 15a, contour interval is 10. In Figures 15b and 15c, contour interval is 0.25. Contours larger than 0.5 or less than -0.5 are shaded. Solid lines are for contours greater than or equal to zero, and dotted lines are for contours less than zero.

related to the increased meridional temperature gradients in the middle and upper troposphere in CAM2O due to the large warm bias produced in its simulated temperature field in the tropics and subtropics. Larger meridional temperature gradients lead to stronger westerlies. These westerly biases are significantly reduced in CAM2M, consistent with its improved temperature field (Figure 17c). It is also noted that the rather large westerly bias near 10°N and easterly bias near 10°S in the lower troposphere in CAM2O are also slightly reduced in CAM2M.

6. Summary and Discussions

[35] In this study, we implemented the convective triggering mechanism proposed by *Xie and Zhang* [2000] in CAM2 in order to reduce the too frequent convection in the original model during the warm season over land. The performance of the CAM2 with the modified convective triggering mechanism was evaluated under the CAPT framework, in which the climate model is run in NWP mode with the initial data obtained from the ERA-40 reanalysis. A series of 24-hour forecasts were conducted by initiating the model every day at 0000 UT for 30 days from 18 June 1997 to 17 July 1997. Model results are compared with the observations collected from the ARM 1997 summer IOP at the SGP site, the global GPCP precipitation data and ISCCP satellite cloud data, and the ERA-40 reanalyses. At the ARM SGP site we have shown that CAM2M significantly reduces the frequency of model convection when compared to CAM2O, generally in better agreement with the ARM observations. This results in a more realistic simulation of other important atmospheric fields, such as temperature, moisture, clouds, radiation, surface temperature, and surface sensible and latent heat fluxes. When compared to CAM2O, for example, CAM2M showed a much smaller warm/dry bias in its simulated temperature and moisture fields; the overestimation of high clouds and underestimation of surface temperature were substantially reduced; and surface energy budgets are closer to the ARM observations. Even with the obvious improvements, however, CAM2M still missed and underestimated a number of strong convective events and failed to accurately

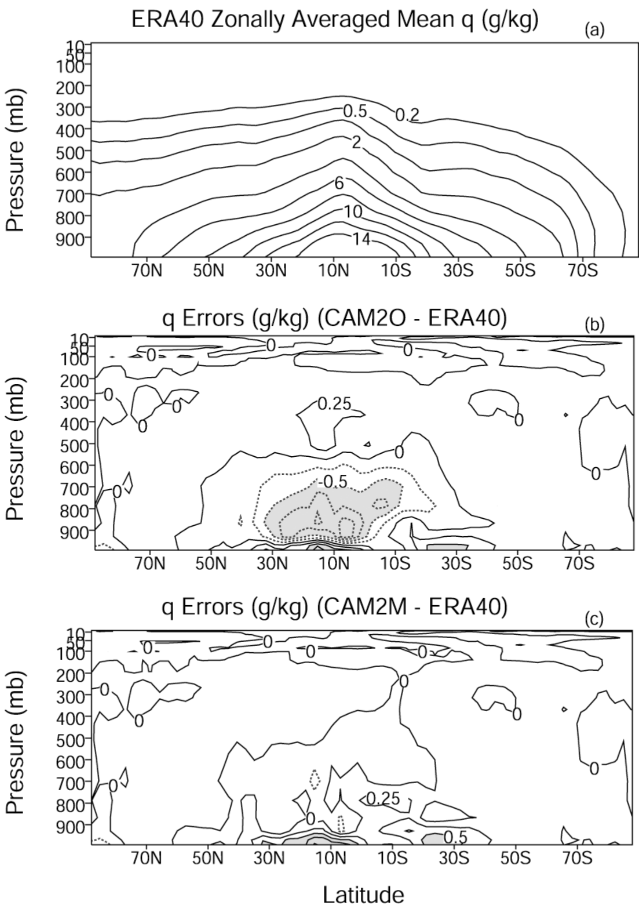

Figure 16. (a) Zonally averaged mean moisture over the 30 days from ERA-40 and the differences (b) between CAM2O and ERA-40 and (c) between CAM2M and ERA-40. Units are g kg^{-1}. In Figure 16a, contours are 0.2, 0.5, 1, 2, 4, 6, 8, 10, 12, and 14. In Figures 16b and 16c, contour interval is 0.25. Contours larger than 0.5 or less than -0.5 are shaded. Solid lines are for contours greater than or equal to zero, and dotted lines are for contours less than zero.

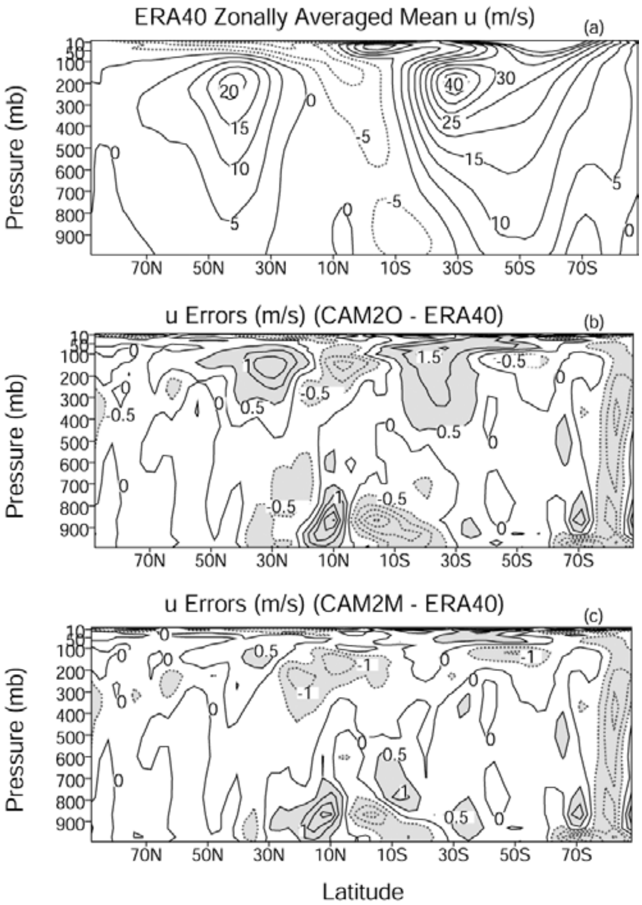

Figure 17. (a) Zonally averaged mean zonal wind over the 30 days from ERA-40 and the differences (b) between CAM2O and ERA-40 and (c) between CAM2M and ERA-40. Units are m s^{-1}. In Figure 17a, contour interval is 5. In Figures 17b and 17c, contour interval is 0.5. Contours larger than 0.5 or less than -0.5 are shaded. Solid lines are for contours greater than or equal to zero, and dotted lines are for contours less than zero.

capture the observed diurnal variation of precipitation. This is partially due to errors in the model-produced large-scale dynamic fields and requires further study.

[36] The distributions over the continental United States and the globe of the simulated precipitation and high clouds in CAM2M showed an excellent agreement with the observations. The principal features of the observed precipitation and tropical high clouds were well reproduced, both in spatial pattern and in magnitude. In contrast, CAM2O generally overestimates these fields mainly because of the overestimation of the frequency of convection occurrence.

[37] The zonally averaged mean temperature is generally colder in the troposphere in CAM2M than it is in CAM2O because of less convection triggered in CAM2M. Significant improvements have been shown in the middle and upper troposphere between 30°N and 10°S, where the large warm bias in CAM2O is greatly reduced. Consistent with the improvements in the temperature, CAM2M substantially reduced this large dry bias in the lower troposphere between 30°N and 10°S in CAM2O. In addition, the westerlies in the upper troposphere between 30°N and 40°N and between 10°S and 30°S are also improved in CAM2M.

[38] It is interesting to note that the biases shown here in the CAM2 short-range weather forecasts are also the systematic errors in the CAM2 climate simulations. Examples are the extremely overestimated high clouds in the tropics in the vicinity of the ITCZ and the spurious precipitation maximum to the east of the Rockies. This suggests that the systematic errors in both climate simulation and weather forecasts could be due to the same reasons. Thus running the climate model in NWP mode can help us to identify what model deficiencies cause the systematic climate errors. The reduction of these errors in CAM2M shown in this study suggests a potential link between the climate errors and problems associated with model cumulus parameterizations.

[39] This study represents an example of how to efficiently transfer improved parameterizations made from SCM tests to three-dimensional climate models before they can be used to improve climate simulations. It has shown that the modified trigger is suitable to use globally. Evaluation of the new triggering mechanism in climate simulations is currently underway. Preliminary results from a 10-year climate simulation using CAM2M show a number of desirable improvements in the simulation of surface precipitation, clouds, and other fields, particularly over tropical and subtropical regions, when compared to CAM2O. Some systematic climate errors, such as the unrealistic double Intertropical Precipitation Zone and the excessive high clouds produced in CAM2O, are noticeably reduced. Details about the climate simulations will be reported as part of a separate study.

[40] **Acknowledgments.** We thank the three anonymous reviewers, whose valuable comments helped to clarify and improve the paper. This research was performed under the auspices of the U.S. Department of Energy (DOE) Office of Science, Biological and Environmental Research by the University of California Lawrence Livermore National Laboratory under contract W-7405-Eng-48. Work at SUNY Stony Brook was supported by ARM grant DE-FG02-98ER62570 and was also supported by NSF under grant ATM9701950. The ARM data were obtained from the Atmospheric Radiation Measurement (ARM) Program, supported by the DOE Office of Science. We would like to thank James Hack from NCAR for several useful discussions on the revised convective triggering function. We thank John Yio for his great help in processing the ARM data. Support from the LLNL CAPT team is greatly appreciated. The Climate Data Analysis Tools (CDAT) that were developed in the Program for Climate Model Diagnosis and Intercomparison (PCMDI) were used to perform our analyses.

References

Ackerman, T. P., and G. M. Stokes (2003), The Atmospheric Radiation Measurement Program, *Phys. Today*, *56*, 38–44.

Arakawa, A., and W. H. Schubert (1974), Interaction of a cumulus cloud ensemble with the large-scale environment, Part I, *J. Atmos. Sci.*, *31*, 674–701.

Barnes, S. L. (1964), A technique for maximizing details in numerical map analysis, *J. Appl. Meteorol.*, *3*, 396–409.

Collins, W. D., et al. (2003), Description of the NCAR Community Atmosphere Model (CAM2), 171 pp., Natl. Cent. for Atmos. Res., Boulder, Colo.

Coquard, J., et al. (2004), Simulations of western U.S. surface climate in 15 global climate models, *Clim. Dyn.*, in press.

Dai, A. (2001), Global precipitation and thunderstorm frequencies: Part II. Diurnal variations, *J. Clim.*, *14*, 1112–1128.

Dai, A., and K. T. Trenberth (2004), The diurnal cycle and its depiction in the Community Climate System Model, *J. Clim.*, *17*, 930–951.

Dai, A., F. Giorgi, and K. E. Trenberth (1999), Observed and model simulated precipitation diurnal cycle over the contiguous United States, *J. Geophys. Res.*, *104*, 6377–6402.

Duffy, P. B., B. Govindasamy, J. P. Iorio, J. Milovich, K. R. Sperber, K. E. Taylor, M. F. Wehner, and S. L. Thompson (2003), High-resolution simulations of global climate: Part 1. Present climate, *Clim. Dyn.*, *21*, 371–390.

Fritsch, J. M., and C. F. Chappell (1980), Numerical prediction of convectively driven mesoscale pressure systems: Part I. Convective parameterization, *J. Atmos. Sci.*, *37*, 1722–1733.

Ghan, S. J., et al. (2000), An intercomparison of single column model simulations of summertime midlatitude continental convection, *J. Geophys. Res.*, *105*, 2091–2124.

Hack, J. J. (1994), Parameterization of moist convection in the National Center for Atmopsheric Research Community Climate (CCM2), *J. Geophys. Res.*, *99*, 5551–5568.

Huffman, G. J., R. F. Adler, M. M. Morrissey, D. T. Bolvin, S. Curtis, R. Joyce, B. McGavock, and J. Susskind (2001), Global precipitation at one-degree daily resolution from multisatellite observations, *J. Hydrometeorol*, *2*, 36–50.

Kain, J. S., and J. M. Fritsch (1993), Convective parameterization for mesoscale models: The Kain-Fritsch scheme, the representation of cumulus convection in numerical models, *Meteorol. Monogr.*, *46*, 165–170.

Kiehl, J. T., J. J. Hack, G. B. Bonan, B. A. Boville, D. L. Williamson, and P. J. Rasch (1998), The National Center for Atmospheric Research Community Climate Model: CCM3, *J. Clim.*, *11*, 1131–1149.

Klein, S. A., and C. Jakob (1999), Validation and sensitivities of front clouds simulated by the ECMWF model, *Mon. Weather Rev.*, *127*, 2514–2531.

Kuo, H. L. (1965), On formation and intensification of tropical cyclones through latent heat release by cumulus convection, *J. Atmos. Sci.*, *22*, 40–63.

Kuo, H. L. (1974), Further studies of the parameterization of the influence of cumulus convection on large-scale flow, *J. Atmos. Sci.*, *31*, 1232–1240.

Lin, W. Y., and M. H. Zhang (2004), Evaluation of clouds and their radiation effects simulated by the NCAR Community Atmospheric Model CAM2 against satellite observations, *J. Clim.*, in press.

Minnis, P., W. L. Smith, D. P. Garber, J. K. Ayers, and D. R. Doeling (1995), Cloud properties derived from GOES-7 for spring 1994 ARM Intensive Observing Period using version 1.0.0 of ARM satellite data analysis program, *NASA Ref. Publ., 1366*, 59 pp.

Phillips, T. J., et al. (2004), Evaluating parameterizations in general circulation models: Climate simulation meets weather prediction, *Bull. Am. Meteorol. Soc.*, in press.

Rogers, R., and J. M. Fritsch (1996), A general framework for convective trigger functions, *Mon. Weather Rev.*, *124*, 2438–2452.

Rossow, W. B., A. W. Walker, D. Beuschel, and M. Roiter (1996), International Satellite Cloud Climatology Project (ISCCP) description of new cloud datasets, *WMO/TD 737*, 115 pp., World Clim. Res. Programme, Int. Counc. of Sci. Unions, Geneva.

Stokes, G. M., and S. E. Schwartz (1994), The Atmospheric Radiation Measurement (ARM) Program: Programmatic background and design of the cloud and radiation test bed, *Bull. Am. Meteorol. Soc.*, *75*, 1202–1221.

Wang, J., and D. A. Randall (1994), The moist available energy of a conditionally unstable atmosphere: II. Further analysis of the GATE data, *J. Atmos. Sci.*, *51*, 703–710.

Webb, M., C. Senior, S. Bony, and J. J. Morcrette (2001), Combining ERBE and ISCCP data to assess clouds in the Hadley Centre, ECMWF and LMD atmospheric climate models, *Clim. Dyn.*, *17*, 905–922.

White, P. W. (Ed.) (2001), FULL-POS postprocessing and interpolation, in *IFS Documentation Part VI: Technical and Computational Procedures (CY23R4)*, chap. 2, Eur. Cent. for Medium-Range Weather Forecasts, Reading, UK.

Xie, S. C. (1998), Single-column modeling: Methodology and application to the evaluation of cumulus convection schemes in GCMs, Ph.D. thesis, 126 pp., State Univ. of New York at Stony Brook.

Xie, S. C., and M. H. Zhang (2000), Impact of the convective triggering function on single-column model simulations, *J. Geophys. Res.*, *105*, 14,983–14,996.

Xie, S. C., et al. (2002), Intercomparison and evaluation of cumulus parameterizations under summertime midlatitude continental conditions, *Q. J. R. Meteorol. Soc.*, *128*, 1095–1135.

Xie, S. C., R. T. Cederwall, M. Zhang, and J. Yio (2003), Comparison of SCM and CSRM forcing data derived from the ECMWF model and from objective analysis at the ARM SGP, *J. Geophys. Res.*, *108*(D16), 4499, doi:10.1029/2003JD003541.

Zhang, G. J. (2002), Convective quasi-equalibrium in midlatitude continental environment and its effect on convective parameterization, *J. Geophys. Res.*, *107*(D14), 4220, doi:10.1029/2001JD001005.

Zhang, G. J., and N. A. McFarlane (1991), Convective stabilization in midlatitudes, *Mon. Weather Rev.*, *119*, 1915–1928.

Zhang, G. J., and N. A. McFarlane (1995), Sensitivity of climate simulations to the parameterization of cumulus convection in the Canadian Climate Center general circulation model, *Atmos. Ocean*, *33*, 407–446.

Zhang, M. H., and J. L. Lin (1997), Constrained variational analysis of sounding data bases on column-integrated budgets of mass, heat, moisture, and momentum: Approach and application to ARM measurements, *J. Atmos. Sci.*, *54*, 1503–1524.

Zhang, M. H., J. L. Lin, R. T. Cederwall, J. J. Yio, and S. C. Xie (2001), Objective analysis of ARM IOP Data: Method and sensitivity, *Mon. Weather Rev.*, *129*, 295–311.

J. S. Boyle, R. T. Cederwall, G. L. Potter, and S. Xie, Atmospheric Science Division, Lawrence Livermore National Laboratory, L-103, Livermore, CA 94550, USA. (boyle@pcmdi.llnl.gov; rcederwall@llnl.gov; gpotter@llnl.gov; xie2@llnl.gov)

W. Lin and M. Zhang, Marine Sciences Research Center, State University of New York at Stony Brook, Stony Brook, NY 11794-5000, USA. (wuyin.lin@msrc.sunysb.edu; mzhang@atmsci.msrc.sunysb.edu)